1-2015

Role of Antenna Modes and Field Enhancement in Second Harmonic Generation from Dipole Nanoantennas

Domenico de Ceglia
Charles M. Bowden Research Center

Maria Antonietta Vincenti
Charles M. Bowden Research Center

Costantino De Angelis
Università degli Studi di Brescia

Andrea Locatelli
Università degli Studi di Brescia

Joseph W. Haus
University of Dayton, jhaus1@udayton.edu

See next page for additional authors

Author(s)
Domenico de Ceglia, Maria Antonietta Vincenti, Costantino De Angelis, Andrea Locatelli, Joseph W. Haus, and Michael Scalora

Role of antenna modes and field enhancement in second harmonic generation from dipole nanoantennas

Domenico de Ceglia,[1,*] Maria Antonietta Vincenti,[1] Costantino De Angelis,[2] Andrea Locatelli,[2] Joseph W. Haus,[3] and Michael Scalora[4]

[1]*National Research Council - AMRDEC, Charles M. Bowden Research Center, Redstone Arsenal, AL 35898, USA*
[2]*Dipartimento di Ingegneria dell'Informazione, Università degli Studi di Brescia, Brescia 25123, Italy*
[3]*Electro-Optics Program, University of Dayton, Dayton, OH 45469-2951, USA*
[4]*Charles M. Bowden Research Center, AMRDEC, RDECOM, Redstone Arsenal, AL 35898-5000, USA*
[*]*domenico.deceglia@us.army.mil*

Abstract: We study optical second harmonic generation from metallic dipole antennas with narrow gaps. Enhancement of the fundamental-frequency field in the gap region plays a marginal role on conversion efficiency. In the symmetric configuration, i.e., with the gap located at the center of the antenna axis, reducing gap size induces a significant red-shift of the maximum conversion efficiency peak. Either enhancement or inhibition of second-harmonic emission may be observed as gap size is decreased, depending on the antenna mode excited at the harmonic frequency. The second-harmonic signal is extremely sensitive to the asymmetry introduced by gap's displacements with respect to the antenna center. In this situation, second-harmonic light can couple to all the available antenna modes. We perform a multipolar analysis that allows engineering the far-field SH emission and find that the interaction with quasi-odd-symmetry modes generates radiation patterns with a strong dipolar component.

OCIS codes: (160.4330) Nonlinear optical materials; (190.2620) Harmonic generation and mixing; (250.5403) Plasmonics.

References and links

1. P. Bharadwaj, B. Deutsch, and L. Novotny, "Optical antennas," Adv. Opt. Photon. **1**(3), 438–483 (2009).
2. S. A. Maier, *Plasmonics: Fundamentals and Applications* (Springer, 2007).
3. P. J. Schuck, D. P. Fromm, A. Sundaramurthy, G. S. Kino, and W. E. Moerner, "Improving the mismatch between light and nanoscale objects with gold bowtie nanoantennas," Phys. Rev. Lett. **94**(1), 017402 (2005).
4. P. Biagioni, D. Brida, J.-S. Huang, J. Kern, L. Duò, B. Hecht, M. Finazzi, and G. Cerullo, "Dynamics of four-photon photoluminescence in gold nanoantennas," Nano Lett. **12**(6), 2941–2947 (2012).
5. M. Castro-Lopez, D. Brinks, R. Sapienza, and N. F. van Hulst, "Aluminum for nonlinear plasmonics: Resonance-driven polarized luminescence of Al, Ag, and Au nanoantennas," Nano Lett. **11**(11), 4674–4678 (2011).
6. M. Lippitz, M. A. van Dijk, and M. Orrit, "Third-harmonic generation from single gold nanoparticles," Nano Lett. **5**(4), 799–802 (2005).
7. B. Lamprecht, J. Krenn, A. Leitner, and F. Aussenegg, "Resonant and off-resonant light-driven plasmons in metal nanoparticles studied by femtosecond-resolution third-harmonic generation," Phys. Rev. Lett. **83**(21), 4421–4424 (1999).
8. M. Danckwerts and L. Novotny, "Optical frequency mixing at coupled gold nanoparticles," Phys. Rev. Lett. **98**(2), 026104 (2007).
9. S. Kim, J. Jin, Y.-J. Kim, I.-Y. Park, Y. Kim, and S.-W. Kim, "High-harmonic generation by resonant plasmon field enhancement," Nature **453**(7196), 757–760 (2008).
10. N. Bloembergen and P. S. Pershan, "Light Waves at the Boundary of Nonlinear Media," Phys. Rev. **128**(2), 606–622 (1962).
11. J. E. Sipe, V. C. Y. So, M. Fukui, and G. I. Stegeman, "Analysis of second-harmonic generation at metal surfaces," Phys. Rev. B **21**(10), 4389–4402 (1980).

#223474 - $15.00 USD Received 19 Sep 2014; revised 25 Nov 2014; accepted 1 Dec 2014; published 23 Jan 2015

12. M. Scalora, M. A. Vincenti, D. de Ceglia, V. Roppo, M. Centini, N. Akozbek, and M. J. Bloemer, "Second- and third-harmonic generation in metal-based structures," Phys. Rev. A **82**(4), 043828 (2010).
13. J. I. Dadap, J. Shan, and T. F. Heinz, "Theory of optical second-harmonic generation from a sphere of centrosymmetric material: small-particle limit," J. Opt. Soc. Am. B **21**(7), 1328–1347 (2004).
14. A. Benedetti, M. Centini, C. Sibilia, and M. Bertolotti, "Engineering the second harmonic generation pattern from coupled gold nanowires," J. Opt. Soc. Am. B **27**(3), 408–416 (2010).
15. A. Benedetti, M. Centini, M. Bertolotti, and C. Sibilia, "Second harmonic generation from 3D nanoantennas: on the surface and bulk contributions by far-field pattern analysis," Opt. Express **19**(27), 26752–26767 (2011).
16. K. Thyagarajan, S. Rivier, A. Lovera, and O. J. F. Martin, "Enhanced second-harmonic generation from double resonant plasmonic antennae," Opt. Express **20**(12), 12860–12865 (2012).
17. J. L. Coutaz, M. Neviere, E. Pic, and R. Reinisch, "Experimental study of surface-enhanced second-harmonic generation on silver gratings," Phys. Rev. B Condens. Matter **32**(4), 2227–2232 (1985).
18. M. Larciprete, A. Belardini, M. Cappeddu, D. De Ceglia, M. Centini, E. Fazio, C. Sibilia, M. Bloemer, and M. Scalora, "Second-harmonic generation from metallodielectric multilayer photonic-band-gap structures," Phys. Rev. A **77**(1), 013809 (2008).
19. M. Kauranen and A. V. Zayats, "Nonlinear plasmonics," Nat. Photonics **6**(11), 737–748 (2012).
20. B. Canfield, S. Kujala, K. Jefimovs, J. Turunen, and M. Kauranen, "Linear and nonlinear optical responses influenced by broken symmetry in an array of gold nanoparticles," Opt. Express **12**(22), 5418–5423 (2004).
21. R. Czaplicki, M. Zdanowicz, K. Koskinen, J. Laukkanen, M. Kuittinen, and M. Kauranen, "Dipole limit in second-harmonic generation from arrays of gold nanoparticles," Opt. Express **19**(27), 26866–26871 (2011).
22. H. Husu, B. Canfield, J. Laukkanen, B. Bai, M. Kuittinen, J. Turunen, and M. Kauranen, "Local-field effects in the nonlinear optical response of metamaterials," Metamaterials (Amst.) **2**(2-3), 155–168 (2008).
23. B. K. Canfield, H. Husu, J. Laukkanen, B. Bai, M. Kuittinen, J. Turunen, and M. Kauranen, "Local Field Asymmetry Drives Second-Harmonic Generation in Non-Centrosymmetric Nanodimers," Nano Lett. **7**(5), 1251–1255 (2007).
24. J. Butet, S. Dutta-Gupta, and O. J. F. Martin, "Surface second-harmonic generation from coupled spherical plasmonic nanoparticles: Eigenmode analysis and symmetry properties," Phys. Rev. B **89**(24), 245449 (2014).
25. X. Meng, R. R. Grote, J. I. Dadap, N. C. Panoiu, and R. M. Osgood, "Engineering metal-nanoantennae/dye complexes for maximum fluorescence enhancement," Opt. Express **22**(18), 22018–22030 (2014).
26. P. Mühlschlegel, H. J. Eisler, O. J. F. Martin, B. Hecht, and D. W. Pohl, "Resonant Optical Antennas," Science **308**(5728), 1607–1609 (2005).
27. J. Berthelot, G. Bachelier, M. Song, P. Rai, G. Colas des Francs, A. Dereux, and A. Bouhelier, "Silencing and enhancement of second-harmonic generation in optical gap antennas," Opt. Express **20**(10), 10498–10508 (2012).
28. A. Slablab, L. Le Xuan, M. Zielinski, Y. de Wilde, V. Jacques, D. Chauvat, and J. F. Roch, "Second-harmonic generation from coupled plasmon modes in a single dimer of gold nanospheres," Opt. Express **20**(1), 220–227 (2012).
29. J. Butet, K. Thyagarajan, and O. J. F. Martin, "Ultrasensitive Optical Shape Characterization of Gold Nanoantennas Using Second Harmonic Generation," Nano Lett. **13**(4), 1787–1792 (2013).
30. M. A. Vincenti, S. Campione, D. de Ceglia, F. Capolino, and M. Scalora, "Gain-assisted harmonic generation in near-zero permittivity metamaterials made of plasmonic nanoshells," New J. Phys. **14**(10), 103016 (2012).
31. D. de Ceglia, S. Campione, M. A. Vincenti, F. Capolino, and M. Scalora, "Low-damping epsilon-near-zero slabs: Nonlinear and nonlocal optical properties," Phys. Rev. B **87**(15), 155140 (2013).
32. D. Maystre, M. Neviere, and R. Reinisch, "Nonlinear polarisation inside metals: A mathematical study of the free-electron model," Appl. Phys., A Mater. Sci. Process. **39**(2), 115–121 (1986).
33. E. D. Palik and G. Ghosh, *Handbook of optical constants of solids* (Academic Press, 1998).
34. A. D. Rakic, A. B. Djurisic, J. M. Elazar, and M. L. Majewski, "Optical Properties of Metallic Films for Vertical-Cavity Optoelectronic Devices," Appl. Opt. **37**(22), 5271–5283 (1998).
35. J. Rudnick and E. A. Stern, "Second-Harmonic Radiation from Metal Surfaces," Phys. Rev. B **4**(12), 4274–4290 (1971).
36. R. Rojas, F. Claro, and R. Fuchs, "Nonlocal response of a small coated sphere," Phys. Rev. B Condens. Matter **37**(12), 6799–6807 (1988).
37. C. David and F. J. García de Abajo, "Spatial Nonlocality in the Optical Response of Metal Nanoparticles," J. Phys. Chem. C **115**(40), 19470–19475 (2011).
38. C. Ciracì, R. T. Hill, J. J. Mock, Y. Urzhumov, A. I. Fernández-Domínguez, S. A. Maier, J. B. Pendry, A. Chilkoti, and D. R. Smith, "Probing the Ultimate Limits of Plasmonic Enhancement," Science **337**(6098), 1072–1074 (2012).
39. M. Weber and A. Liebsch, "Density-functional approach to second-harmonic generation at metal surfaces," Phys. Rev. B Condens. Matter **35**(14), 7411–7416 (1987).
40. J. E. Sipe, D. J. Moss, and H. M. van Driel, "Phenomenological theory of optical second- and third-harmonic generation from cubic centrosymmetric crystals," Phys. Rev. B Condens. Matter **35**(3), 1129–1141 (1987).
41. A. Alù and N. Engheta, "Input Impedance, Nanocircuit Loading, and Radiation Tuning of Optical Nanoantennas," Phys. Rev. Lett. **101**(4), 043901 (2008).

#223474 - $15.00 USD Received 19 Sep 2014; revised 25 Nov 2014; accepted 1 Dec 2014; published 23 Jan 2015

42. A. Locatelli, C. De Angelis, D. Modotto, S. Boscolo, F. Sacchetto, M. Midrio, A.-D. Capobianco, F. M. Pigozzo, and C. G. Someda, "Modeling of enhanced field confinement and scattering by optical wire antennas," Opt. Express **17**(19), 16792–16800 (2009).
43. R. Esteban, A. G. Borisov, P. Nordlander, and J. Aizpurua, "Bridging quantum and classical plasmonics with a quantum-corrected model," Nat. Commun. **3**, 825 (2012).
44. J. W. Haus, D. de Ceglia, M. A. Vincenti, and M. Scalora, "Quantum conductivity for metal-insulator-metal nanostructures," J. Opt. Soc. Am. B **31**(2), 259–269 (2014).
45. J. W. Haus, D. de Ceglia, M. A. Vincenti, and M. Scalora, "Nonlinear quantum tunneling effects in nanoplasmonic environments: two-photon absorption and harmonic generation," J. Opt. Soc. Am. B **31**(6), A13–A19 (2014).
46. J. Aizpurua, G. W. Bryant, L. J. Richter, F. J. García de Abajo, B. K. Kelley, and T. Mallouk, "Optical properties of coupled metallic nanorods for field-enhanced spectroscopy," Phys. Rev. B **71**(23), 235420 (2005).
47. M. Liu, T.-W. Lee, S. K. Gray, P. Guyot-Sionnest, and M. Pelton, "Excitation of Dark Plasmons in Metal Nanoparticles by a Localized Emitter," Phys. Rev. Lett. **102**(10), 107401 (2009).
48. M. A. Vincenti, D. de Ceglia, M. Grande, A. D'Orazio, and M. Scalora, "Tailoring Absorption in Metal Gratings with Resonant Ultrathin Bridges," Plasmonics **8**(3), 1445–1456 (2013).
49. A. Locatelli, "Analysis of the optical properties of wire antennas with displaced terminals," Opt. Express **18**(9), 9504–9510 (2010).
50. J. Petschulat, J. Yang, C. Menzel, C. Rockstuhl, A. Chipouline, P. Lalanne, A. Tüennermann, F. Lederer, and T. Pertsch, "Understanding the electric and magnetic response of isolated metaatoms by means of a multipolar field decomposition," Opt. Express **18**(14), 14454–14466 (2010).
51. J. D. Jackson, *Classical Electrodynamics* (Wiley, 1999).
52. R. E. Raab and O. L. de Lange, *Multipole Theory in Electromagnetism* (Oxford, 2005).
53. P. Grahn, A. Shevchenko, and M. Kaivola, "Electromagnetic multipole theory for optical nanomaterials," New J. Phys. **14**(9), 093033 (2012).

1. Introduction

The manipulation of light with optical nanoantennas [1] may unlock a plethora of new opportunities for microscopy and spectroscopy devices, enhanced photovoltaic cells, and for a large variety of optical and electro-optical applications that are typically limited by diffraction. Efficient transformation of propagating light waves into highly confined fields, and vice versa, is mediated by the excitation of plasmon resonances localized at the surface of metallic nanostructures. Nanoantennas may enhance nonlinear processes initiated in the surrounding media, in the bulk of the metal, and at the interfaces. The most relevant boosting mechanism for nonlinear interactions in metallic nanostructures is usually the field enhancement induced by surface plasmon resonances and by the lightning-rod effect [2]. Noble metals display large intrinsic third and higher-odd-order nonlinear susceptibilities. Enhanced multiphoton photoluminescence from noble metals has been experimentally observed in bowtie nanoantennas [3], in gap [4] and rod [5] antennas. Conversion efficiency of parametric nonlinear processes involving cubic and higher-order nonlinearities, such as third harmonic generation [6, 7], four-wave mixing [8], and high-harmonic generation [9] is substantially boosted by the field enhancement of isolated or arrayed nanoantennas when these structures are designed to resonate at the pump and/or at the harmonic frequencies. On the other hand, second-harmonic (SH) generation in centrosymmetric media such as noble metals is forbidden in the electric-dipole approximation and is governed solely by quadrupole and higher-order bulk response, and by dipole contributions due to symmetry breaking at the interfaces [10]. In the hydrodynamic theory of free electrons in metals, the quadratic nonlinear response arises from Lorentz and Coulomb electromagnetic forces, convective forces and quantum pressure [11, 12]. Several strategies have been proposed to promote the SH signal produced by these forces. These approaches are usually based on the excitation of surface waves, for example using nanoparticles [13] and nanoantennas [14–16], coupling to surface plasmon polaritons on planar metallic surfaces [11] or phase matching to complex modes of metallic gratings [17]. An alternative way to efficiently access the quadratic nonlinear response of metal without resorting to surface plasmons involves impedance matching techniques, as demonstrated by Larciprete et al. [18] in metal-dielectric, photonic band gap structures. SH generation from metal nanoparticles is extremely sensitive to the shape and symmetry of the particle [19]. The role of defects, symmetry and higher-multipole

#223474 - $15.00 USD Received 19 Sep 2014; revised 25 Nov 2014; accepted 1 Dec 2014; published 23 Jan 2015

effects in SH generation from nanoparticles have been discussed in several works [20–24]. The importance of engineering the geometry of plasmonic nanostructures has been recently highlighted for the enhancement of radiation from fluorescent molecules [25].

In this paper we investigate SH light scattered by dipole nanoantennas pumped with plane wave illumination. Dipole antennas, which consist of two metallic arms separated by a tiny gap, are attractive for their extraordinary ability to enhance the local field in the gap region. Their linear optical properties have been extensively investigated [26]. It has been experimentally proven that the SH signal from symmetric dipole antennas may be suppressed when the gap size is reduced [27], despite the strong enhancement of the fundamental-frequency (FF) field in the gap region [28]. A pronounced sensitivity to small geometrical perturbations has been predicted by observing modulations in the quadrupolar far-field pattern of SH light scattered by symmetric dipole antennas [29]. This property may be suitable for shape characterization of nanoparticles. Enhancement of SH light has been observed in doubly resonant antennas formed by two small gaps properly displaced along the antenna axis [16]. The symmetric dipole antenna has been also studied as a platform to evaluate the relative weights of surface and bulk contributions to SH generation [15]. Different regimes have been identified, in which either surface or bulk responses may be dominant. It has been shown that no *a priori* assumption can be made concerning the origin of SH light and the strength of surface and bulk nonlinearities; hence inclusion of all the relevant nonlinear contributions is the safest approach. Here we clarify the role of antenna resonances and field enhancement in SH generation from both symmetric and asymmetric dipole antennas, when the full quadratic nonlinear response (both surface and bulk contributions) of metal is considered. We observe that the field enhancement in the gap region has minimal effect on the SH scattering efficiency and far field, which remain inherently quadrupolar in symmetric dipole antennas. However, we find that the presence of the gap in the antenna center, even for gap sizes of only a few nanometers, drastically blue-shifts the peak of maximum SH scattering efficiency. Our results clarify why either SH enhancement or inhibition may be observed as gap size is reduced [27, 28]. Either effect is possible depending on the available antenna mode at the SH frequency. We then go on to show that a displacement of the gap with respect to the antenna center induces dipolar and octupolar responses at the SH frequency, therefore allowing the SH light to efficiently couple to quasi-odd charge-symmetry modes. We provide a multipolar representation of SH generation in order to explain the peculiar behavior of asymmetric dipole antennas.

2. Field enhancement and second harmonic sources

For simplicity we consider dipole antennas placed in free-space, made by silver strips with translational invariance along the z direction. The structures are excited by TM-polarized light so that the electric field is on the x-y plane. Linear and nonlinear properties of metallic strips are analogous to those found in their three-dimensional counterparts, i.e., rod antennas. However, the system under investigation, illustrated in Fig. 1, may be studied in two dimensions instead of three, with significant savings of computational resources when nonlinear sources are included. The strip width w = 10 nm and length L_{ant} = 300 nm are kept constant, while the gap size s and the gap displacement d with respect to the center of the antenna are varied in order to evaluate the sensitivity of SH radiation to pump field enhancement and antenna symmetry. The elongated shape (L_{ant}/w = 30) provides a large number of antenna modes in the frequency range of interest (visible and near infrared), therefore it is instrumental in determining the impact of these modes on SH scattering. All the corners of the antenna are rounded with a radius of curvature of 1.5 nm to avoid diverging fields. SH light is only a small fraction of linearly scattered light so that a perturbative approach may be adopted. First we solve the linear electromagnetic problem at the FF using a frequency-domain finite-element solver (COMSOL) and then we use the calculated fields to define the SH current sources and solve the problem at the SH frequency by using the same

#223474 - $15.00 USD Received 19 Sep 2014; revised 25 Nov 2014; accepted 1 Dec 2014; published 23 Jan 2015

approach reported in [30, 31]. SH radiation is due to nonlinear forces acting on both free and bound electrons in metal. Presently we neglect nonlinear contributions of bound electrons, since they are usually weaker with respect to convective and quantum pressure forces acting on free electrons [12].

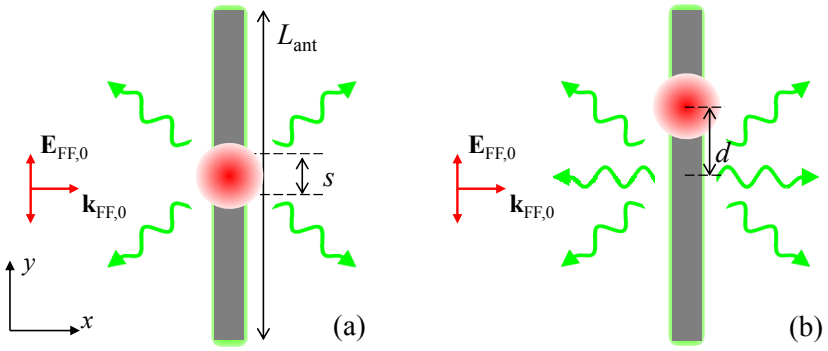

Fig. 1. Plane wave illumination of symmetric (a) and asymmetric (b) dipole nanoantennas. $(\mathbf{E})_{FF,0}$ is the input FF electric field polarized along the antenna axis (y-axis). The input wavevector $\mathbf{k}_{FF,0}$ points in the x direction. The red shadow symbolizes the FF field enhancement in the middle of the gap. Green arrows indicate scattering of SH light.

The current density source of SH light may be expressed as the superposition of two contributions, one coming from the volume of the antenna, $\mathbf{J}_{vol}$, the other, $\mathbf{J}_{surf}$, located at the metal surface. Following the method outlined in [14, 30, 32], these currents can be explicitly related to the FF electric field and to the free electron hydrodynamic parameters as follows:

$$\hat{\mathbf{n}}\cdot\mathbf{J}_{surf} = i\frac{n_0 e^3}{2m_*^2}\frac{3+\varepsilon_{FF}}{(\omega+i\gamma_0)^2(2\omega+i\gamma_0)}E_{FF,\perp}^2 \tag{1}$$

$$\hat{\mathbf{t}}\cdot\mathbf{J}_{surf} = i\frac{2n_0 e^3}{m_*^2}\frac{1}{(\omega+i\gamma_0)^2(2\omega+i\gamma_0)}E_{FF,\perp}E_{FF,//} \tag{2}$$

$$\mathbf{J}_{vol} = \frac{n_0 e^3}{m_*^2}\frac{1}{\omega(\omega+i\gamma_0)(2\omega+i\gamma_0)}\left[\frac{\gamma_0}{\omega+i\gamma_0}(\mathbf{E}_{FF}\cdot\nabla)\mathbf{E}_{FF} - \frac{i}{2}\nabla(\mathbf{E}_{FF}\cdot\mathbf{E}_{FF})\right] \tag{3}$$

where $n_0 = 4.96\times10^{28}$ m^{-3} is the free electrons density in silver assuming the effective electron mass is $m_* = m_e = 9.11\times10^{-31}$ Kg, e is the elementary charge, $\gamma_0 = 7.28\times10^{13}$ s^{-1} is the electron gas collision frequency in silver, ε_{FF} is the bulk-silver, relative permittivity at the FF taken from Palik [33] and interpolated with one Drude and five Lorentz oscillators as in [34], and ω the angular frequency of the FF field. Moreover, $\mathbf{E}_{FF}$ is the FF electric field, $\hat{\mathbf{n}}$ and $\hat{\mathbf{t}}$ are unit vectors pointing in directions outward normal and tangential to the metallic surface, respectively. $E_{FF,\perp}$ and $E_{FF,//}$ are the normal (evaluated inside the metal region) and tangential components of the FF electric field in the local boundary coordinate system defined by $\hat{\mathbf{n}}$ and $\hat{\mathbf{t}}$, respectively. We note that the source component $\hat{\mathbf{n}}\cdot\mathbf{J}_{surf}$ in Eq. (1) is dominant for this particular geometry, in the sense that it would be sufficient to describe qualitatively the SH scattering properties. However in our calculations we also retain the sources in Eqs. (2) and (3) in order to provide more accurate, quantitative predictions of SH efficiencies.

#223474 - $15.00 USD Received 19 Sep 2014; revised 25 Nov 2014; accepted 1 Dec 2014; published 23 Jan 2015

In Eqs. (1)-(3) we neglect the inherently nonlocal nature of light interaction with free electrons and adopt the local approximation, i.e., we assume that the free electrons' Fermi velocity $v_F << \omega / q$, where q is the inverse of the characteristic length of variation of the electromagnetic field [35]. Typical phenomena associated with the free electrons nonlocality are slight perturbations on the linear response, in the form of a blue shift and quenching of plasmonic resonances [36, 37], and limitations of field enhancement in sub-nanometer gaps between metallic objects [38]. Nonlocality, as well as surface phenomena related to realistic roughness and spill-out of electrons at metal interfaces, may also affect the nonlinear response [39]. However simple models like the one adopted here usually provide good qualitative agreement with experiments, properly describing near- and far-field properties of SH light, but may be quantitatively improved by introducing phenomenological parameters [40]. The FF excitation is a homogeneous plane wave travelling in the *x*-direction and polarized along the dipole antenna axis (*y*-axis), as shown in Fig. 1.

In Fig. 2 we report spectra of electric field enhancement in the symmetric dipole antenna of Fig. 1(a) as a function of gap size *s*. The enhancement is evaluated in the center of the gap region with respect to the amplitude of the input plane wave E_0. Regardless of gap position, the input field magnification is fairly uniform in the gap region, while the enhancement level depends weakly on the displacement *d*.

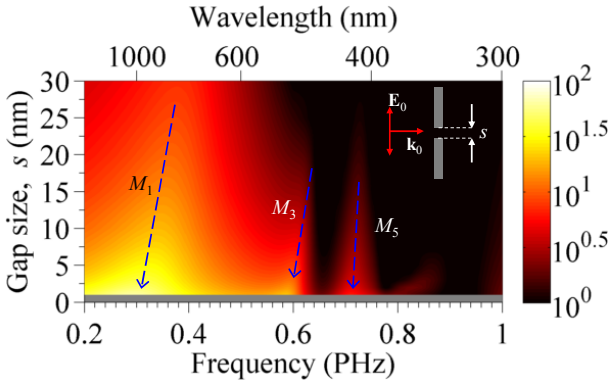

Fig. 2. Field enhancement $|(\mathbf{E})|/E_0$ spectra evaluated at the gap center of symmetric antennas (as illustrated in Fig. 1(a)) as a function of gap size *s*. Input field is polarized along the antenna axis, as shown in the inset.

The peaks in the field enhancement spectra are resonances due to plane wave excitation of modes with odd-charge symmetry (defined with labels M_1, M_3, M_5), sometimes referred to as *bright* modes. Here the definition of odd/even charge symmetry refers to the charge distribution across the L_{ant}-long antenna; specifically, in odd/even modes charges of opposite/same sign are located at the two extremities of the antenna. The gap acts as a nanocapacitor with capacitance per unit length $C = \varepsilon_0 w / s$ inversely proportional to the gap size *s*, [41, 42] hence the resonances' red-shift with decreased gap sizes. We direct the interested reader to [41, 42] for details on the circuit-theory model of the antenna. The charge accumulation at the metallic edges facing the gap promotes a field enhancement that increases with smaller gaps. For example, with an input frequency of ~0.3 PHz, close to the first odd mode (M_1), the electric field amplitude in a 1-nm-thick gap is magnified by a factor of ~60 with respect to the source field. In this paper, we deliberately avoid gap sizes smaller than 1 nm, for which quantum effects in the gap region may not be neglected [43]. Quantum tunneling currents induced in sub-nm gaps increase absorption losses at the FF and may add quadratic and cubic, nonlinear sources that are predicted to interfere with the metal nonlinearities [44, 45]. We will discuss this regime in a separate work.

#223474 - $15.00 USD Received 19 Sep 2014; revised 25 Nov 2014; accepted 1 Dec 2014; published 23 Jan 2015

Field enhancement is usually the most important requirement for efficient nonlinear interactions with nanophotonic structures. A generally accepted notion is that nanoantennas with smaller gaps provide larger nonlinear conversion efficiencies, as suggested in [28] for SH generation. However, it was recently demonstrated that SH generation may be inhibited when gap size is reduced [27]. The observed decrease of SH radiation is ascribed to the intrinsic, nonradiative (*dark*) and quadrupolar nature of SH light scattered by symmetric gap antennas. Since the structure is centrosymmetric, the SH electric field component parallel to the antenna's axis is forced to form a zero in the gap center, thus mimicking a quadrupole-like source. Here we show that the introduction of a gap, at least in the classical picture of the problem, does not alter the level of SH scattering efficiency, but shifts the maximum peak from the second-order, even-charge-symmetry mode (M_4) to the lowest-order, even mode (M_2). We then clarify the role of antenna modes in both symmetric and non-symmetric dipole nanoantennas, supporting our conclusions with a multipolar analysis of the SH generated signal.

3. Antenna modes

Antenna modes may be studied with several techniques. Here we use two different approaches: (i) plane wave excitation in order to assess the antenna response as a receiver for the pump at the FF; (ii) point-dipole excitation to evaluate the radiation efficiency at the SH frequency.

3.1 Modes of symmetric dipole antennas

In the symmetric configuration the gap is located in the center of the antenna axis, i.e., $d = 0$. We first analyze linear extinction efficiencies for plane wave illumination in the frequency range 0.2-1 PHz (wavelengths in the range 300-1500 nm). We report normalized extinction cross section spectra for different values of the gap size s in Fig. 3(a). The normalized extinction cross section $\mathrm{ECS} = \left(\int_\ell \mathbf{S}_{\mathrm{sca}} \cdot \hat{\mathbf{n}} dl + \int_\Omega Q dS \right) \Big/ \left(L_{\mathrm{ant}} I_0 \right)$ is calculated by integrating the scattered, time averaged Poynting vector $\mathbf{S}_{\mathrm{sca}}$ on a circle surrounding the antenna, and the Joule heating rate $Q = 1/2 \omega \varepsilon_0 \, \mathrm{Im}\left(\varepsilon_m \right) \left| \mathbf{E} \right|^2$ in the metal volume. In the expressions above, $\hat{\mathbf{n}}$ is the unit vector normal to the integration circle, $\mathbf{E}$ is the electric field phasor, $I_0 = 1/2 \varepsilon_0 c E_0^2$ is the irradiance of the input plane wave, ε_0 and c are the permittivity and speed of light in free space, respectively, $\mathrm{Im}\left(\varepsilon_m \right)$ the imaginary part of the metal relative permittivity, and E_0 the amplitude of the input plane wave. The radius of the integration circle is much larger than the excitation wavelength in order to obtain a far-field measure of the scattering efficiency. For symmetry reasons, plane waves polarized along the antenna axis are able to excite only modes with large electric dipole moment and, as a consequence, odd charge-symmetry distribution along the antenna, i.e., modes M_1, M_3, M_5 … These modes are sometimes referred to as *bonding* or *bright* modes. The distribution of the electric field component E_y, which is uniformly enhanced in the gap, is compatible with charge accumulation of opposite signs on the metallic edges facing the gap region [46]. Decreasing gap size from s = 30 nm to s = 1 nm results in a significant red-shift of the resonances and, as mentioned in the previous section, in a strong increase of field enhancement in the gap. Nevertheless the extinction efficiency remains almost unchanged (see Fig. 3) against variations of gap size s. From this analysis it is clear that the pump field, which is launched as a plane wave, will interact mostly with odd-charge-symmetry modes with a strong electric field enhancement in the gap. On the other hand, SH radiation generates from currents induced on the antenna itself (both on the surface and in the volume of metal) and it can couple, in principle, to any available antenna mode. A complete map of the modes supported by the antenna is retrieved from the dipole excitation scheme illustrated in the inset of Fig. 3(b). We follow the procedure outlined in [47], in which

#223474 - $15.00 USD Received 19 Sep 2014; revised 25 Nov 2014; accepted 1 Dec 2014; published 23 Jan 2015

a point emitter (quantum dot) with electric dipole with moment $\mathbf{p}_0$ aligned with the antenna axis (y-axis) feeds the antenna from a subwavelength distance (10 nm) below the bottom edge of the antenna, as described in the inset of Fig. 3(b).

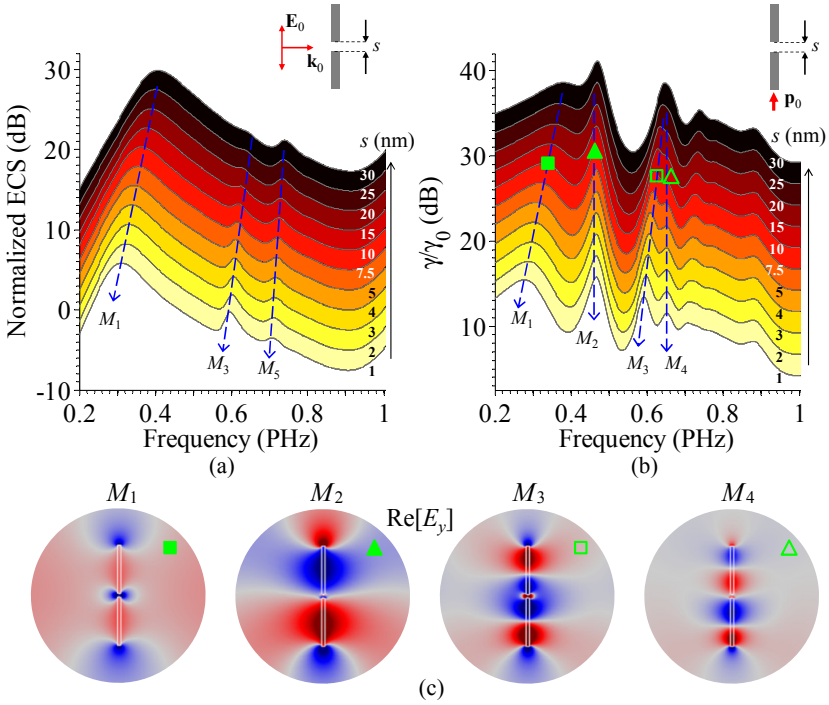

Fig. 3. (a) Normalized extinction cross section, ECS, as a function of input frequency and gap size. The inset shows the excitation scheme. (b) Spectra of radiative decay of a dipole emitting in proximity of a symmetric dipole antenna for different gap sizes. The dipole's location (10 nm away from the lower edge of the antenna) is shown in the inset. For illustration purposes, an offset of 2.5 dB is used to distinguish spectra corresponding to different gap sizes. (c) Distribution of the real part of the electric field component parallel to the antenna axis (Re[E_y]) for the first four modes supported by the dipole nanoantenna. The color scale is normalized to the field maximum for each mode. The modes are probed with the dipole excitation technique using a gap size s = 10 nm, at frequencies 0.34 PHz for mode M_1, 0.46 PHz for M_2, 0.6 PHz for M_3 and 0.68 PHz for M_4, as indicated by the green triangles and squares in (b).

Proceeding in this fashion one is able to excite modes with arbitrary charge-symmetry. In this case we measure the normalized radiation decay rate, defined as $\gamma_r / \gamma_0 = \int_\ell \mathbf{S}_{\text{ant}} \cdot \mathbf{n} dl / \int_\ell \mathbf{S}_0 \cdot \mathbf{n} dl$, where $\mathbf{S}_{\text{ant/0}}$ is the time-averaged Poynting vector due to dipole emission in the presence/absence of the antenna. The observed peaks in the spectra are due to interactions with both odd- (M_1, M_3, M_5) and even-charge-symmetry (M_2, M_4) modes. Charges of same/opposite sign are induced on the two metallic edges facing the gap region in even/odd modes [46]. In Fig. 3(c) we report the real part of the E_y field distribution for the first four modes, $M_{1\text{-}4}$. In odd-charge symmetry modes the field component E_y displays an odd number of local maxima/minima along the antenna axis and a strong peak inside the gap due to charge accumulation. Conversely, E_y shows an even number of maxima/minima along the antenna axis for even-charge-symmetry modes with a zero-crossing in the middle of the gap region: no field build-up is allowed. y-polarized plane waves can excite even modes of the nanoantenna when system symmetry is perturbed by the close proximity to larger scatterers, as demonstrated in metal gratings with ultrathin bridges [48]. In the framework of hybridization theory, odd modes are defined as low-energy bonding modes, while even modes

#223474 - $15.00 USD Received 19 Sep 2014; revised 25 Nov 2014; accepted 1 Dec 2014; published 23 Jan 2015

are high-energy antibonding modes. Interestingly, for gaps much smaller than antenna length the frequency of even modes is insensitive to gap size variations, as the interaction with the gap capacitive load is virtually suppressed. As observed with the plane wave excitation scheme, bonding modes undergo a substantial red-shift for smaller gap sizes due to charge accumulation on the gap capacitance. Another significant difference between modes of opposite parity concerns the far-field patterns. Odd modes have a net dipole moment. Thus, the far-field shows two main lobes orthogonal to the antenna axis, while the vanishing dipole moment of even modes results in a quadrupole-like far-field pattern. For this reason, bonding modes are sometimes called "bright", whereas antibonding modes are referred to as "near-field" or "dark" modes. However, the bright/dark nomenclature may also be misleading. For example, in the next section we will show that SH light is scattered with larger efficiency when coupled to dark modes of symmetric antennas, since the SH sources overlaps well with even-charge symmetry modes. The picture complicates for asymmetric antennas, where SH scattering is sensitive to the degree of asymmetry. Then, gap displacement forms modes with quasi-even and quasi-odd symmetry. We will show that both types of modes may be dominant ("bright") depending on the position of the gap along the antenna axis.

3.2 Modes of asymmetric dipole antennas

A thorough investigation of asymmetric dipole antennas can be found in [49], where a circuit theory approach is adopted to describe the linear properties of the structure. Here we analyze the effects of a displaced gap on the antenna resonances, for both plane wave excitation and dipole excitation. We fix gap size to s = 10 nm, while the gap displacement d is varied between 0 and 120 nm. Similarly to symmetric antennas, antenna modes are probed with both the plane wave and the point dipole feeding schemes. Spectra of normalized extinction efficiency and radiation rates are mapped as functions of d in Fig. 4(a) and 4(b), respectively. Even though the lack of symmetry prevents the existence of purely even- and odd-charge-symmetry modes, yet the gap-displaced antenna supports modes with quasi-even and quasi-odd symmetry. For a given gap size, the resonances associated with these modes, labeled $\tilde{M}_{1-4}$ in Fig. 4, peak at frequencies close to those found for modes M_{1-4} in the symmetric case. The frequency shift with respect to the symmetric case depends on gap displacement. In contrast to the symmetric case, the structural asymmetry allows a y-polarized plane wave to excite both quasi-odd and quasi-even modes (Fig. 4(a)). As expected, resonances associated with quasi-even modes and higher-order, quasi-odd modes are more pronounced in the radiation spectra of the point dipole source (Fig. 4(b)). The scattering or radiation efficiency remains unaltered for the dominant mode $\tilde{M}_1$, whose peak is only red-shifted by increasing the gap displacement d. The resonant peak of higher-order modes is modulated both in frequency and amplitude by variations of d. From this analysis we may surmise that the antenna interaction with the pump field will be governed by the quasi-odd $\tilde{M}_1$ mode, while SH radiation may couple to quasi-even and quasi-odd modes with radiation efficiency modulated by the gap displacement d. An important difference with respect to the symmetric case regards the field localization and charge accumulation around the gap region. Purely even/odd modes of symmetric antennas support only charges of same/opposite sign at the metallic edges facing the gap region, resulting in a zero/maximum E_y field at the center of the gap, as shown in Fig. 3(c). This is not the case for modes $\tilde{M}_{1-4}$ of the asymmetric antenna. In fact, quasi-even modes may support strong field localization in the gap with a generally asymmetric charge distribution around the gap region, as shown in Fig. 4(c) for the fields of the $\tilde{M}_2$ and $\tilde{M}_4$ modes when the gap displacement is d = 50nm. On the other hand, the gap capacitance may be virtually shorted in quasi-odd modes if the gap position corresponds to a zero of the E_y field distribution along the antenna axis. Under these circumstances a small

#223474 - $15.00 USD Received 19 Sep 2014; revised 25 Nov 2014; accepted 1 Dec 2014; published 23 Jan 2015

accumulation of charges with the same sign occurs at the metallic edges surrounding the gap, resulting in a weak coupling between the two arms of the antenna, a typical behavior of the so-called "antibonding" modes.

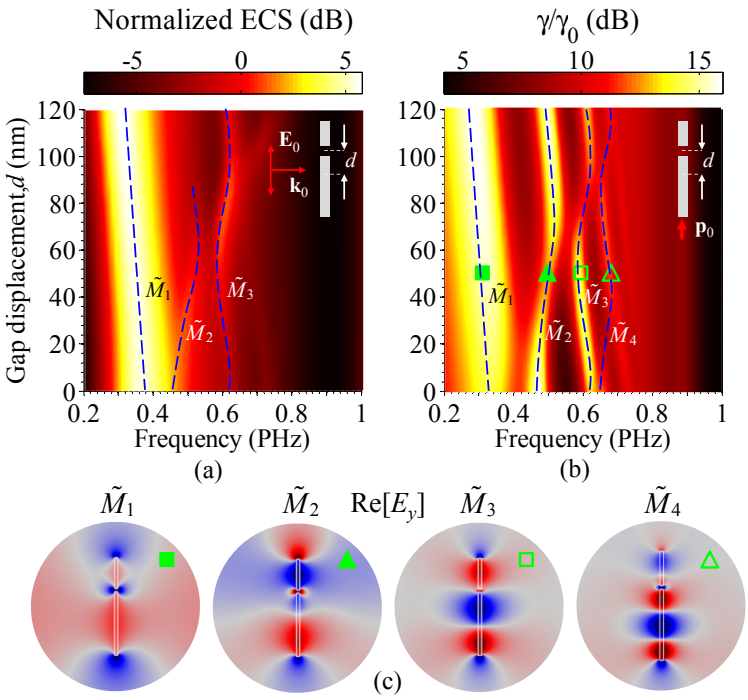

Fig. 4. (a) Normalized extinction cross section, ECS, as a function of input frequency and gap displacement *d*. The inset shows the plane wave excitation scheme. (b) Spectra of radiative decay of a dipole emitting in proximity of symmetric dipole antenna. The dipole's location (10 nm far from the lower edge of the antenna) is shown in the inset. The blue curves are guides for the eye to indicate the antenna modes excited by a plane wave (a) and a point dipole (b). (c) Distribution of the real part of the electric field component parallel to the antenna axis (Re[E_y]) for the first four modes supported by the asymmetric dipole nanoantenna. The modes are probed with the dipole excitation technique using a displacement d = 50 nm, at frequencies 0.3 PHz for mode $\tilde{M}_1$, 0.5 PHz for $\tilde{M}_2$, 0.6 PHz for $\tilde{M}_3$ and 0.68 PHz for $\tilde{M}_4$, as indicated by the green triangles and squares in (b).

4. SH generation in symmetric and asymmetric nanoantennas

We first consider scattering from the symmetric antenna. In the above analysis we showed that optimal interaction with the nanoantenna in terms of scattering and field enhancement in the gap is achieved when the mode M_1 is excited by a plane wave polarized along the antenna axis (*y*-direction), regardless of gap size *s* and displacement *d*. Therefore, we tune the FF in the range 0.2-0.5 PHz to exploit the broad resonance associated with this mode. Pump field enhancement decreases from ~60 (frequency ~0.3 PHz and s = 1 nm) to ~6 (frequency ~0.4 PHz and s = 30 nm), as shown in Fig. 2. SH scattering efficiency is evaluated as a function of pump frequency and gap size by using the approach outlined in section 2. We define efficiency as $\eta_{\mathrm{SH}} = \int_{\ell} \mathbf{S}_{\mathrm{sca,SH}} \cdot \hat{\mathbf{n}} dl \Big/ \left(L_{\mathrm{ant}} I_0\right)$; $\mathbf{S}_{\mathrm{sca,SH}}$ is the time-averaged, Poynting vector at the SH frequency and pump irradiance is $I_0 = 1\,\mathrm{GW/cm^2}$. SH conversion efficiency η_{SH} is mapped on a logarithmic color scale in Fig. 5(a). We find several peaks in the SH scattering spectra. Each peak originates from SH-light coupling to an even-charge-symmetry mode of the nanoantenna (M_{2n}, n = 1, 2, ….) These are the only "bright" modes for SH generation in

#223474 - $15.00 USD Received 19 Sep 2014; revised 25 Nov 2014; accepted 1 Dec 2014; published 23 Jan 2015

the symmetric configuration of the antenna. Mode M_2 creates an efficiency peak at a SH frequency of ~0.46 PHz (FF ~0.23 PHz), mode M_4 at ~0.64 PHz (FF ~0.32 PHz).

In Fig. 5(b) we plot the distributions of the real part of the SH field $E_{SH,y}$ for these two peaks in order to show the symmetry compatibility of the generated signal with respect to modes M_2 and M_4. As already observed in the linear radiation rate spectra (Fig. 3(b)), the resonance frequency of even modes is barely sensitive to gap size, at least for gaps much smaller than the antenna length ($s << L_{ant}$). This trend may also be identified in the SH generation spectra. However the SH scattering efficiency on the two main peaks undergoes a significant modulation as gap size decreases. In particular, mode M_4 produces the largest SH signal for $s > 5$ nm, while mode M_2 turns out to be more important as s decreases.

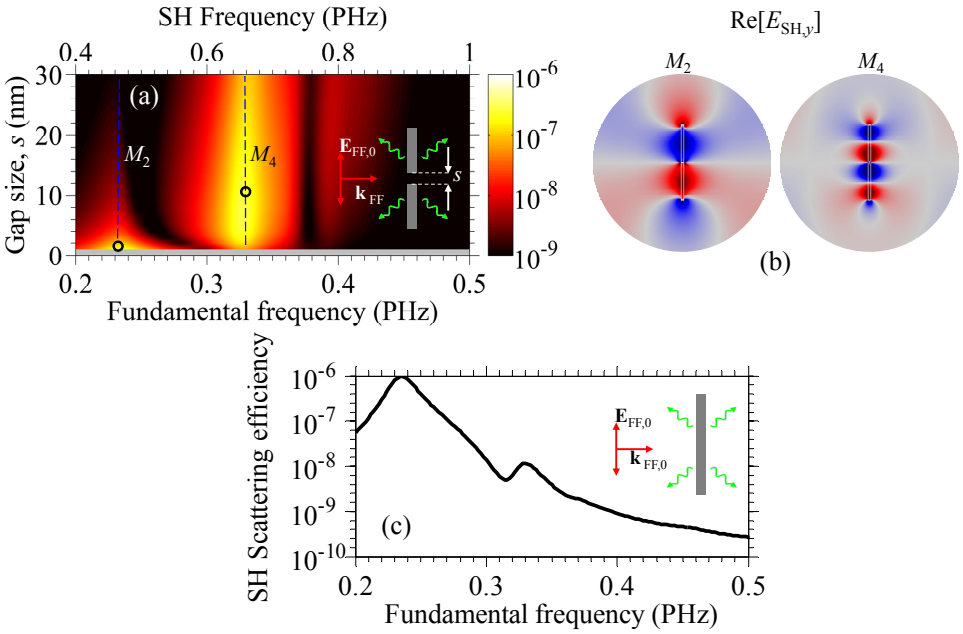

Fig. 5. (a) SH conversion efficiency η_{SH} for the symmetric ($d = 0$) dipole nanoantenna as a function of FF and SH frequency, and gap size s. The color map is reported on a logarithmic scale. (b) E_y field distributions for SH light when mode M_2 is excited by a pump tuned at ~0.23 PHz and mode M_4 is excited by a pump tuned at ~0.32 PHz. (c) Spectrum of SH conversion efficiency η_{SH} for the nanoantenna without gap ($s = 0$, as shown in the inset).

We remark that field enhancement inside the gap is increasingly large for decreasing gap sizes (see Fig. 2) but plays a minimal role in the SH generation process. This becomes clear by looking at the conversion efficiency reduction at the peak associated with mode M_4. However, the efficiency peak due to mode M_2 gains intensity when gap size is reduced, suggesting an improvement apparently related to the increased field enhancement in the gap region. Nevertheless, we find that the peak due to mode M_2 is actually the dominant one when the nanoantenna has no gap at all ($s = 0$), confirming that field enhancement in the gap is not important for SH generation. Indeed, the SH efficiency spectrum of the gapless structure, shown in Fig. 5(c), seems the natural extension of the efficiency map in Fig. 5(a) as s approaches zero, in terms of both frequency position of the peaks and scattering efficiency levels. This means that the SH signal is sensitive to the geometry and symmetry of the structure rather than field enhancement in the gap. Our results indicate the existence of two distinct regimes: for gaps in the range 1-3 nm, the SH light emitted by the structure is almost indistinguishable from that radiated by a gapless nanoantenna of total length L_{ant} (see Fig.

#223474 - $15.00 USD Received 19 Sep 2014; revised 25 Nov 2014; accepted 1 Dec 2014; published 23 Jan 2015

5(c)), for which the lowest, and dominant, even mode is M_2; for gaps larger than 3 nm, the structure tends to emit SH radiation like two separated nanoantennas with lengths $L_{ant}/2$. The dominant mode for each of these $L_{ant}/2$-long antennas is the mode M_4 of the L_{ant}-long dipole antenna. In other words, the only significant, nonlinear effect induced by the gap appears for gap sizes larger than 5 nm and manifests itself as a decoupling of the two arms of the dipole antenna. In this regime, the two arms of the dipole antenna, each having length $\approx L_{ant}/2$, radiate SH light as if they were isolated. Therefore, the maximum scattering efficiency is achieved at the frequency of mode M_4 of the L_{ant}-long dipole antenna, which is virtually identical to the frequency of mode M_2 of each $L_{ant}/2$-long arm.

The reason why scattered SH light is unable to benefit from the large field enhancement inside the gap is probably better understood by investigating the induced nonlinear currents. The largest current source is the surface term $\mathbf{J}_{surf}$, which depends on the pump electric fields at the antenna surface (see Eq. (1)). The electric field has a large discontinuity at the metal surface, due to the significant permittivity mismatch with respect to vacuum. $\mathbf{J}_{surf}$ is thus proportional to the intensity of the pump field on the metal side of the interface $|\mathbf{E}^{-}_{FF}|^2$, which is much smaller than the field on the vacuum side (see Eqs. (1) and (2)). In Fig. 6 we report field enhancement on the metal surface of the antenna's upper arm for the two main peaks of the SH efficiency map in Fig. 5(a): (i) gap size s = 1 nm and FF of 0.23 PHz, where mode M_2 enhances SH light, and (ii) gap size s = 10 nm with FF of 0.32 PHz, where SH light is coupled to mode M_4. The field on the lower arm is not reported since it has specular symmetry due to the geometry and excitation configurations. While field enhancement on the vacuum side of the interface, $|\mathbf{E}^{+}_{FF}|/E_{FF,0}$, increases in the gap region as the gap size is reduced from 10 nm to 1 nm, as shown in Fig. 6(a), it remains fairly low and almost unchanged on the metal side (see $|\mathbf{E}^{-}_{FF}|/E_{FF,0}$ in Fig. 6(b)). Moreover, the average field enhancement on the metal side is even larger in the case with gap s = 10 nm than in the case with s = 1 nm due to the smaller silver permittivity at 0.32 PHz. This explains the essential insensitivity of SH light to field enhancement in the gap.

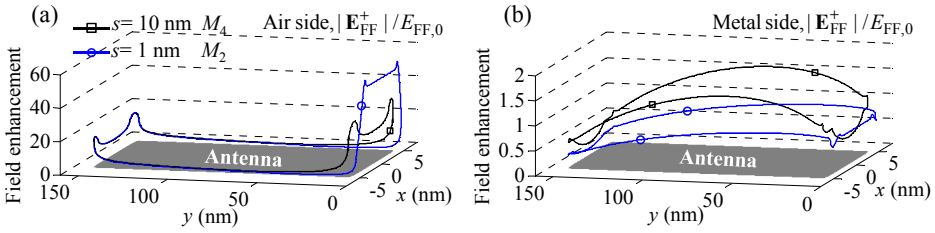

Fig. 6. Pump field enhancement on the metal surface evaluated on the air side (a) and metal side (b). The black (blue) curve refers to an antenna with a gap size of s = 1 nm (s = 10 nm) pumped at a frequency of 0.23 PHz (0.32 PHz), where mode M_2 (M_4) enhances SH scattering. The shaded areas represent the approximate location of the metallic antenna.

Next we consider the asymmetric antenna. The gap size is set at s = 10 nm and the displacement d varies from 0 to 100 nm. We use the same pumping conditions of the symmetric case, with the FF varying in the range 0.2-0.5 PHz, so that the pump is coupled to quasi-odd mode $\tilde{M}_1$ of the antenna. The spectra of SH scattering efficiency are mapped in Fig. 7(a). We can identify several peaks, each associated with a mode of the asymmetric antenna. The substantial difference from the symmetric case is that SH light is now allowed to interact with quasi-odd-symmetry modes. In Fig. 7(a) we have highlighted three branches (with dashed blue lines), belonging to modes $\tilde{M}_2$, $\tilde{M}_3$ and $\tilde{M}_4$. The signatures of these modes overlap well with those found with the linear analysis by using the dipole excitation

#223474 - $15.00 USD Received 19 Sep 2014; revised 25 Nov 2014; accepted 1 Dec 2014; published 23 Jan 2015

(see the similarity to the blue curves in Fig. 4(b)). Even if the asymmetry introduces only a shallow modulation of SH scattering efficiency, it is enough to make one particular antenna mode dominant over the others, producing efficiency peaks in different frequency ranges depending on the amount of asymmetry (d). For the specific antenna under investigation (with gap size s = 10 nm), mode $\tilde{M}_4$ is dominant for very small gap displacements (d < 20 nm), while mode $\tilde{M}_2$ prevails for very asymmetric structures (d > 80 nm). However, for intermediate gap displacements, the quasi-odd mode $\tilde{M}_3$ produces the largest SH signal. In Fig. 7(b) we show the real part of the E_y field distributions and far field patterns for three points of the map in Fig. 7(a), in order to highlight these three regimes.

While mode $\tilde{M}_2$ and $\tilde{M}_4$ lend SH light a purely quadrupolar response, on the branch pertaining to mode $\tilde{M}_3$ SH light is a superposition of quadrupole and dipole responses, with a prevailing dipolar component, as one can infer by looking at the radiation pattern. Similarly to symmetric antennas, we have verified that field enhancement in the gap plays a minimal role on the SH scattering efficiency of asymmetric dipole antennas. Therefore our results indicate that very small gaps (s < 3 nm) cannot be "seen" by SH light notwithstanding their displacement with respect to the antenna center. Under these circumstances the antenna scatters SH light as if the gap were shorted and the resulting radiation couples mainly to the mode M_2 or $\tilde{M}_2$, producing efficiency spectra similar to that reported in Fig. 5(c) for the gapless structure.

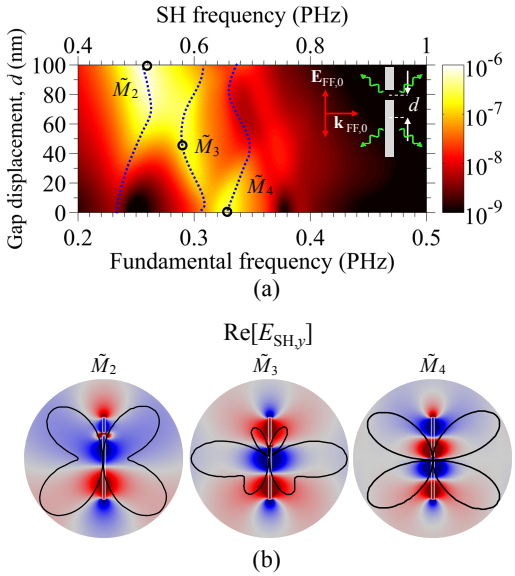

Fig. 7. (a) SH conversion efficiency η_{SH} for asymmetric dipole nanoantenna as a function of fundamental/SH frequency and gap displacement d. The gap size is s = 10 nm. The color map is reported on a logarithmic scale. (b) Distributions of the real part of the $E_{SH,y}$ field for three scenarios: (i) when mode $\tilde{M}_2$ is excited by a pump tuned at ~0.26 PHz with d = 90 nm (left), (ii) mode $\tilde{M}_3$ is excited by a pump tuned at ~0.29 PHz with d = 45 nm, and (iii) mode $\tilde{M}_4 \equiv M_4$ is excited by a pump tuned at ~0.33 PHz with d = 0. The black curves are the SH, far-field radiation patterns associated to the three cases mentioned above.

#223474 - $15.00 USD Received 19 Sep 2014; revised 25 Nov 2014; accepted 1 Dec 2014; published 23 Jan 2015

In order to gain more insight into the multipolar nature of SH light scattered by asymmetric nanoantennas we perform a multipole expansion of the generated field. By adopting the procedure outlined in [50], the scattered magnetic field H_z can be expanded in cylindrical harmonics,

$$H_z = \sum_{m=0}^{\infty} \left[a_m^+ i^m \cos(m\varphi) + a_m^- i^{m+1} \sin(m\varphi) \right] H_m^{(2)}(kr) \tag{4}$$

where $a_m^{\pm}$ are the expansion coefficients, $H_m^{(2)}$ are Hankel functions of the second kind and order m, k the vacuum wavenumber, r the radial distance from the origin (that we set at the center of the antenna axis), and φ the angular position.

The expansion coefficients may be found with two different approaches. One requires the evaluation of overlap integrals between the eigenfunctions ($i^m \cos(m\varphi)$ and $i^{m+1} \sin(m\varphi)$) and the scattered SH far-field [50]. The other approach is based on substituting the nanoantenna with a superposition of Cartesian, point electric multipoles [51, 52] located at the origin, and equating the field produced by these multipoles with the cylindrical expansion in Eq. (2) [50, 53]. Up to the octupole term, the relations between the cylindrical expansion coefficients and the Cartesian multipole moments are as follows:

$$\begin{aligned}
&a_0 = Ak/2(Q_{yx} - Q_{xy}) \\
&a_1^+ = iA[p_y - k^2/4(O_{yyy} - 2O_{xxy} + 3O_{yxx})],\ a_1^- = -A[p_x + k^2/4(2O_{yxy} - O_{xxx} - 3O_{xyy})] \\
&a_2^+ = Ak/2(Q_{yx} + Q_{xy}),\ a_2^- = -iAk/2(Q_{yy} - Q_{xx}) \\
&a_3^+ = -iAk^2/4(O_{yxx} - O_{yyy} + 2O_{xxy}),\ a_3^- = -Ak^2/4(2O_{yxy} - O_{xxx} + O_{xyy})
\end{aligned} \tag{5}$$

where $A = k^3/(4\omega\mu_0\varepsilon_0)$, and $\mathbf{p} = i/\omega \int_\Omega \mathbf{J}(\mathbf{r})\ dS$, $\mathbf{Q} = i/\omega \int_\Omega \mathbf{J}(\mathbf{r})\,\mathbf{r}\ dS$, and $\mathbf{O} = i/(2\omega) \int_\Omega \mathbf{J}(\mathbf{r})\,\mathbf{rr}\ dS$ are the electric dipole, quadrupole and octupole moment tensors, respectively, ω the angular frequency, and $\mathbf{J}(\mathbf{r})$ the distribution of the current density at the SH frequency. Here we neglect magnetic multipoles because of the largely elongated (in the y direction) form-factor of the structure. For the same reason the multipole components p_y, Q_{yy}, and O_{yyy} determine the largest and most significant terms of Eq. (3). We observe that the 0th term of the cylindrical expansion depends on weak quadrupolar terms. The amplitudes of the first cylindrical harmonic $a_1^{\pm}$ are the result of interference between the dipole and octupole fields. The second and third cylindrical harmonics have purely quadrupolar and octupolar origin, respectively. After calculating the multipole moments, one can easily evaluate the contribution of each cylindrical harmonic to the SH scattering efficiency. The total SH scattering efficiency may then be written as $\eta_{SH} = \sum_m \eta_{SH,m}$, where $\eta_{SH,m} = \sqrt{\mu_0/\varepsilon_0}\left(|a_m^+|^2 + |a_m^-|^2\right)/(2kL_{ant}I_0)$ for $m > 0$ and $\eta_{SH,0} = \sqrt{\mu_0/\varepsilon_0}\,|a_0|^2/(kL_{ant}I_0)$ are the efficiencies associated with each order of the cylindrical expansion. Calculations based on overlap integrals and on Cartesian multipoles yields almost the same results.

In Fig. 8 the efficiencies spectra $\eta_{SH,m}$ are mapped for m = 1,2,3 as a function of the gap displacement d, as done in Fig. 7 for the total SH efficiency. The 0-th order efficiency $\eta_{SH,0}$ is negligible for this structure.

Unlike the symmetric antenna, in which SH light is purely quadrupolar, here the asymmetry introduces both a dipole and an octupole SH response. The strengths of these additional contributions are enhanced when the quasi-odd-symmetry mode $\tilde{M}_3$ is excited.

#223474 - $15.00 USD Received 19 Sep 2014; revised 25 Nov 2014; accepted 1 Dec 2014; published 23 Jan 2015

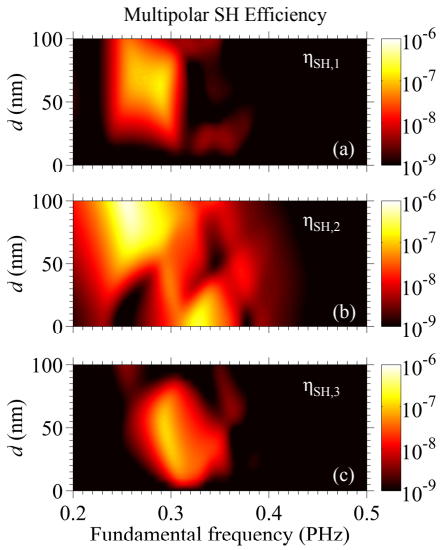

Fig. 8. SH scattering efficiency spectra $\eta_{\mathrm{SH},m}$ mapped for m = 1,2,3 as a function of the gap displacement d. $\eta_{\mathrm{SH},m}$ is the efficiency of the m-th order of cylindrical harmonic expansion.

5. Conclusion

We have studied SH scattering from symmetric and asymmetric metallic dipole nanoantennas with small gaps. We have assessed the roles of field enhancement and antenna modes when both the fundamental and harmonic frequency fields are resonant with the antenna. We find that field enhancement in the gap has minimal impact on the amount of radiated SH light. The only significant effect of gap reduction in symmetric configurations is a strong red-shift of the maximum conversion efficiency: for very small gap sizes (size s < 5 nm) SH emission is maximized at the low-frequency resonance associated with the first even mode, whereas for larger gaps (size s > 5 nm) the SH emission peaks on the high-frequency resonance associated with the second-order even mode. SH light shows a strong sensitivity to asymmetries introduced by gap displacements. The asymmetry enables coupling of SH light to quasi-odd antenna modes, which introduce additional channels to enhance the scattering efficiency. The multipolar analysis reveals that the asymmetry may be engineered to achieve strong dipolar and octupolar radiation components in the SH radiation pattern. Here we have considered only dipole antennas in free space in order to assess unambiguously the nonlinear scattering properties in a perfectly symmetric environment. However, the requirement of a substrate to support the antenna in an experimental setup would inevitably break the system's symmetry. This notwithstanding, we have verified that the presence of a transparent substrate like quartz merely red-shifts the resonances and slightly perturbs SH efficiency, leaving intact our conclusions about field enhancement, antenna modes, and the effects of gap displacement in asymmetric antennas.

Acknowledgments

This research was performed while M. A. Vincenti and D. de Ceglia held a National Research Council Research Associateship award at the U.S. Army AMRDEC. C. De Angelis and A. Locatelli acknowledge financial support from US Army (contract W911NF-13-1-0466, "Engineering second order nonlinear effects in optical antennas") and CARIPLO (contract 2013-0736, "SHAPES - Second-HArmonic Plasmon-Enhanced Sensing").

#223474 - $15.00 USD Received 19 Sep 2014; revised 25 Nov 2014; accepted 1 Dec 2014; published 23 Jan 2015